ARTICLES

Charge Separation in Organic Semiconductor Composites. 2. Study of the Ground State and Low-Lying Excited States Involved

L. Rodriguez-Monge[†]

Service des Materiaux Nouveaux, Université de Mons-Hainaut, 7000 Mons, Belgium

Received: September 4, 1997; In Final Form: March 15, 1998

Composites formed from organic semiconductors are potentially good candidates for the fabrication of photovoltaic cells and other types of optoelectronic devices. In this paper we theoretically investigate by using quantum chemistry methods a model composite formed by poly(*p*-phenylenevinylene) as the major component and perylene as the minor component. This system is simulated by one molecule of the three-ring system of poly(*p*-phenylenevinylene) and a molecule of perylene. The ground state and several low-lying excited states, which include charge-transfer and local excited states, are studied. Geometries and electronic absorption and emission spectra are obtained for the different electronic states under study. The influence of internal coordinate changes on the electronic structure of different low-lying excited states and the relationship of the optoelectronic properties of the system with the corresponding ones of its individual components are analyzed as well. It is seen that some changes in nuclear geometry configurations may introduce important coupling between states, vertical reordering, and altering of the absorption or emission spectra bands and favor charge separation processes.

1. Introduction

Conjugated organic semiconductors are an important class of materials because of their interesting optoelectronic properties, which potentially enable them to be used as the active elements of electronic devices. Recently, their use in photovoltaic cells[1−5] has been investigated. Photovoltaic cells generate electric currents on irradiation with light through the formation of excitons, that is, correlated electron−hole pairs coupled to a local lattice distortion, followed by their dissociation into charges.

The formation of electron−hole (e−h) pairs after photoexcitation is a principal stage in photoconduction. In composites formed from a binary mixture of organic materials, it is unlikely that charge transfer between the components, to form e−h pairs, occurs directly by photoexcitation to an electronic state that has separated charges. In general there are many possible radiative and nonradiative decay mechanisms that can follow photoexcitation in organic solids. The formation of (e−h) pairs may be enhanced either by an electric field or by charge-accepting states provided by an acceptor or a donor molecule in the neighborhood of the excitation. Early-time carrier recombination of the (e−h) pair reduces photoconductivity, and the presence of a donor/acceptor (D/A) interface can enhance the efficiency of photoinduced charge transfer and posterior charge carrier transport. Effective donor/acceptor interfaces may be created between the components provided by composites.

The ground state and the different possible low-lying states of a composite formed by two components, A and B, can be symbolised by BA, B*A, BA*, B^-A^+, and B^+A^-, where they represent the ground state, two local exciton-type states, one localized on component B and the other on component A, respectively, and two e−h pair states, one with the electron transferred from A to B and the other with the electron transferred from B to A, respectively. The energies of these states depend, in general, on the coordinates of all the nuclei in the system, which constitute the potential energy surfaces (PES's) for the electronic states within the Born−Oppenheimer approximation. Each stable state has its corresponding minima on the potential energy surface. Figure 2 shows schematically an example of the PES's of different states.

Electron transfer may be possible between A*B or AB* and A^-B^+ states, and between AB* or A*B and A^+B^- states, depending on the relative variations of the PES with internal and intermolecular nuclear coordinates, and may involve an energy barrier between the initial state and final state. For electron transfer to occur, noninteracting initial and final states should have surfaces that will cross at a multidimensional surface (represented by the solid line in Figure 2). Interaction between initial and final states meanwhile leads to an avoided crossing (represented by dashed lines in Figure 2). For reaction to occur, the donor and the acceptor coordinates in the initial reactant state have to change from its minimum in order to enhance the coupling between their electronic molecular orbitals. A rate constant may be associated with these processes, according to classical transition-state theory. One can apply standard electron-transfer theory (ET)[6] to the study of the charge separation step. We calculate here the internal reorganization energy λ_i,[6−8] which is an important parameter in electron-transfer

[†] Current address: European Bioinformatics Institute (EBI-EMBL), Hinxton Hall (Hinxton), Cambridge CB10 1SD, U.K.

S1089-5647(97)02889-7 CCC: $15.00
Published on Web 05/19/1998

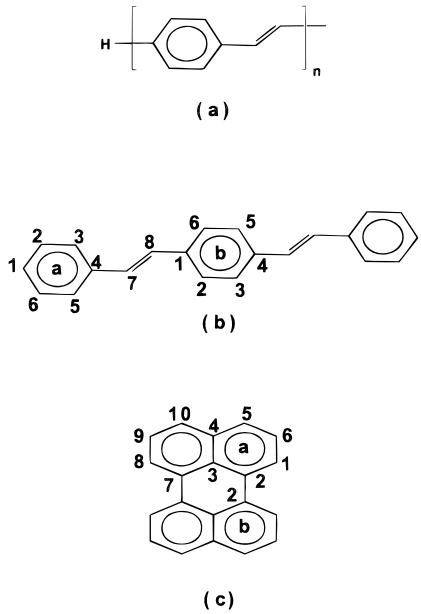

Figure 1. Schematic representation of the unit cell of poly(*p*-phenylenevinylene) (PPV) (a), a molecule of O3PV (b), and a perylene molecule (c).

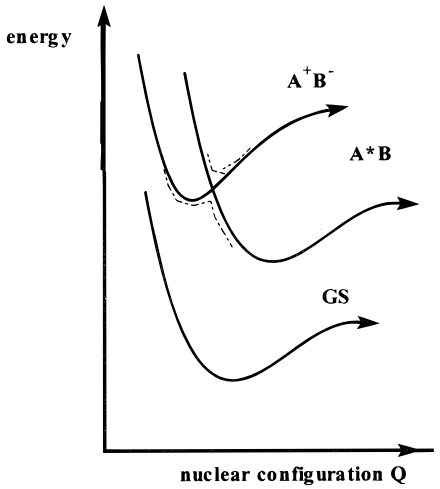

Figure 2. Schematic of the different potential energy surfaces (PES) for the ground state (GS), the exciton (A*B), and the charge-transfer (A^-B^+) electrostatic excited states within the Born−Oppenheimer approximation, where A and B denote the donor and acceptor molecules, respectively. **Q** is the nuclear configuration coordinate, and *E* is the energy.

theory. It is related to the capacity for the system to undergo redox state change.

In the solid state, intermolecular coordinates do not change appreciably during the time in which photoabsorption and energy- or electron-transfer processes take place, and internal coordinates such as torsion angles and bond lengths of the components are important for describing the optoelectronic properties. At any intermolecular spatial arrangement the charge-transfer (CT) and the exciton states surfaces may cross when plotted against coordinates of internal modes of the donor or acceptor. Here we investigate the influence of the internal coordinates within each of the components on the optoelectronic properties of the composite.

The use of quantum chemistry for the study of the electronic and optical properties of these materials can lead to an understanding and prediction of the processes involved in the photophysical behavior of electronic devices fabricated from these materials and thus may help in establishing criteria for the selection of the most suitable composites based on their molecular electronic properties.

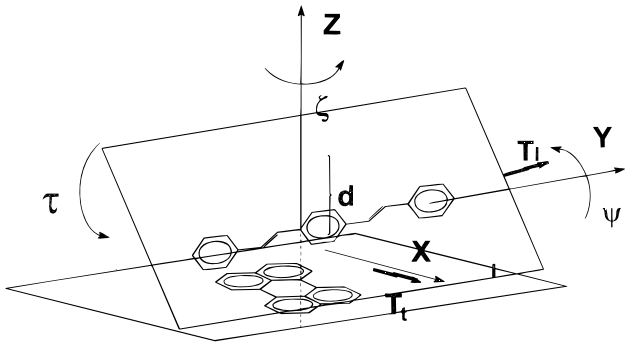

Figure 3. Schematic representation of the spatial disposition of the components of a system formed by one perylene and one PPV3 molecules. The intermolecular coordinates that are varied are **d**, $\mathbf{T}_l$, $\mathbf{T}_t$, ζ, and Ψ, which respectively represent the separation between PER and PPV3, the longitudinal translation vector, the transversal translation vector, the PPV3 rotation around its *Z*-axis, and the PPV rotation around its *Y*-molecular axis.

In this work we are interested in studying the influence of internal coordinate changes on possible photophysical mechanisms affecting the photogeneration of charge carriers in composites formed by organic semiconductors. These are very interesting sort of composites since they can offer large versatility by easy derivatization and modification of their relative composition.

As a model for such composites the system formed by poly(*p*-phenylenevinylene) (PPV) and perylene (PER) as the major and the minor components, respectively, has been chosen. To simulate the PPV, the three-ringed PPV system (O3PV) is used. The PPV unit cell, O3PV, and perylene are shown schematically in parts a, b, and c of Figure 1. PPV has been widely studied both experimentally and theoretically, since some of its derivatives are good candidates for use as the active components in optoelectronic devices.[2,9−13] PER and its derivatives are well-known pigments and have been used extensively in industry as paint pigments and photovoltaic elements in photocopiers and in other electrophotographic applications.[3−5,14] Both PPV and PER can act as acceptors or donors of electrons depending on the medium, the substituents on the molecules, and the relative composition of the composite.

In a previous work[15] we studied the influence of molecular interactions and disorder on different possible photophysical mechanisms for the O3PV+PER system. Several different intermolecular arrangements have very similar stabilities. It was found by using molecular mechanics that the system is stable at all composition ratios and probably has a tendency toward significant intermolecular disorder. It was seen as well that the molecular orbitals (MO) and wave functions of the excited states may be very dependent on the different intermolecular coordinates existing in the disordered material. Disorder will lead to important spatial overlap of state wave functions with different characteristics that would favor effective coupling between states, and thus the occurrence of nonradiative transitions between states.

1.1. Methodology. To establish the relationship between the properties of the material and its individual components, we focus on each of the components of the composite as well as on the O3PV+PER supermolecular system. The geometries for O3PV, PER, and the composite system O3PV+PER (displayed in Figure 3), are optimized for the ground state and

TABLE 1: AM1 and LSDA/3-21G* Bond Length Changes δRx_{ij} Calculated for the O3PV Cation and Anion with Respect to the Ground-State Geometry, $[Q_{(+1)-(0)}]$ and $[Q_{(-1)-(0)}]$, Respectively, between the Anion and Cation, $[Q_{(-1)-(+1)}]$, and the First Excited State and the Ground State, $[Q_{(*)-(0)}]$[a]

	AM1			LSDA/4-31G		LSDA/4-31G*		LSDA/3-21G*	
geom. diff.	$[Q_{(+1)-(0)}]$	$[Q_{(-1)-(0)}]$	$[Q_{(*)-(0)}]$	$[Q_{(+1)-(0)}]$	$[Q_{(-1)-(0)}]$	$[Q_{(+1)-(0)}]$	$[Q_{(-1)-(0)}]$	$[Q_{(+1)-(0)}]$	$[Q_{(-1)-(0)}]$
δRa_{12}	+0.002	+0.000	−0.002	0.004	0.006	0.004	0.006	0.005	0.006
δRa_{23}	−0.003	−0.004	−0.001	−0.005	−0.004	−0.005	−0.004	−0.006	−0.004
δRa_{34}	+0.008	+0.009	−0.000	0.008	0.012	0.008	0.012	0.009	0.013
δRa_{45}	+0.007	+0.008	+0.001	−0.005	−0.002	−0.005	−0.002	0.009	0.013
δRa_{56}	−0.003	−0.004	−0.001	−0.005	−0.002	−0.005	−0.002	−0.005	−0.002
δRa_{61}	+0.002	+0.000	−0.002	0.004	0.006	0.004	0.006	0.005	0.006
δRe_{17}	−0.021	−0.021	−0.001	−0.019	−0.018	−0.019	−0.018	−0.021	−0.020
δRe_{78}	+0.029	+0.023	−0.006	0.020	0.023	0.020	0.023	0.020	0.024
δRe_{81}	−0.036	−0.037	−0.001	−0.021	−0.022	−0.021	−0.022	−0.023	−0.024
δRb_{12}	+0.025	+0.021	−0.004	0.012	0.016	0.012	0.016	0.012	0.013
δRb_{23}	−0.019	−0.020	−0.002	−0.010	−0.007	−0.010	−0.007	−0.010	−0.008
δRb_{34}	+0.022	+0.023	+0.001	0.012	0.012	0.011	0.012	0.013	0.017
δRb_{45}	+0.025	+0.017	−0.008	0.012	0.016	0.012	0.016	0.012	0.013
δRb_{56}	−0.019	−0.017	+0.001	−0.010	−0.007	−0.010	−0.007	−0.010	−0.008

[a] δRx_{ij} is the bond length difference expressed in Å between atoms i and j for the molecule defined in Figure 1b.

low-lying states by means of the semiempirical self-consistent field Austin model 1 (AM1) method[16] with posterior full configuration interaction method within different active spaces consisting of 4, 6, and 10 π orbitals, respectively. To study excited states, we used an active space of 10 molecular orbitals (MO), all of them of π character. A lower number of molecular orbitals in the active space was found to lead to incorrect results. Geometry optimization is performed first without using any geometry restriction and second by imposing planarity on O3PV, since it is found experimentally that in the solid state PPV has very small torsion angles.[17] Both geometrical configurations are used in posterior property calculations.

The transition energies and related intensities for the AM1 geometries of the composite were determined by using the semiempirical intermediate neglect of differential overlap (ZINDO) Hamiltonian with posterior configuration interaction (CI) treatment. The ZINDO parametrization developed by Zerner and co-workers[18] was used here to reproduce the optical absorption spectra of neutral organic molecules. The electronic repulsion terms were calculated with a Mataga−Nishimoto potential.[19] Single and double excitations were performed including the 20 upper occupied and the 20 first unoccupied molecular orbitals.

The available AM1 and ZINDO semiempirical methods use a basis set that is restricted to be minimal (STO-3G[20]). STO-3G quality allows neither an accurate description of the intermolecular interactions of neutral molecules nor those of ion pair systems. A better description for the electronic wave functions of the system requires the use of a more accurate theoretical approach dealing with higher electron correlation and larger basis sets that include polarization functions. Larger basis sets will stabilize in general the excited states. Nevertheless, because of Pauli repulsion in the solid state, the excited states are not as diffuse as they would be in the gas phase, they have very high energies and the system is described better with not too extended basis sets. For such large systems as that of O3PV+PER, we are not able to adopt more correlated methods owing to limitations in computing costs and capabilities, which are even more severe for the study of excited states. Nevertheless, since we are mostly interest in relating trends among the system excited states and not in their absolute values, we use the semiempirical methods in the hope that these will contain the essential physics of these systems and reveal the likely trends.

Additional, geometry optimizations have been done for the individual systems O3PV and PER using density functional theory at the local spin density approximation (LSDA)[21] with basis sets 3-21G*[22] and 4-31G*.[23] Energy calculations on the O3PV+PER AM1 optimized geometries are performed using LSDA with a 3-21G* quality basis set. These results are compared with the results from the AM1 method.

2. Results and Discussion

2.1. Study of Isolated PER and O3PV Components. *2.1.1. Structure.* The AM1 and LSDA/4-31G* geometry changes of the cation, anion, and first singlet excited state, with respect to the neutral ground state of the molecules, are shown in Tables 1 and 2. The bond angles of both O3PV and PER do not change appreciably for the different excited and charged species, compared with the neutral ground state, and these are not shown.

Both the AM1 and LSDA results show similar trends with regards to the changes in bond lengths. LSDA/3-21G* calculations led to similar structures as the LSDA/4-31G* ones but with smaller changes in the ending rings geometry of O3PV.

For both components, O3PV and PER, the geometry changes involved in the processes of excitation, or in adding or removing an electron to the system, lead to a moderate expansion of the rings and a lengthening of the vinyl carbon atoms bond length. The geometry changes are small and extend over the whole system.

The O3PV bond lengths that change most appreciably are the ones of the central ring and those of the vinylene groups. The O3PV cation and anion species have very similar geometries. The O3PV chain dihedral angles formed between the ring and vinylene planes are about 20° for the neutral molecule. Removing an electron diminishes the angles to around 5−6°, and adding an electron leads to almost planar structures.

The most important changes for PER upon adding or removing an electron or by excitation are on the CC bond lengths linking the two napthalene-like moieties constituting PER.

The geometry of a system is related to its corresponding electronic structure. In Figure 3 there is a schematic representation of the the HOMO (highest occupied molecular orbital), HOMO−1 and LUMO (lowest unoccupied molecular orbital) molecular orbitals for O3PV and PER. For O3PV, HOMO and HOMO−1 differ mostly on the central ring of the system. The HOMO is extended over all of the molecule, reflecting the

TABLE 2: AM1 and LSDA/3-21G* Bond Length Changes δRx_{ij} Calculated for the PER Cation and Anion with Respect to the Ground-State Geometry, $[Q_{(+1)-(0)}]$ and $[Q_{(-1)-(0)}]$, Respectively, between the Anion and Cation, $[Q_{(-1)-(+1)}]$, and the First Excited State and the Ground State, $[Q_{(*)-(0)}]$[a]

	AM1				LSDA/3-21G*		
PER	$[Q_{(+1)-(0)}]$	$[Q_{(-1)-(0)}]$	$[Q_{(-1)-(+1)}]$	$[Q_{(*)-(0)}]$	$[Q_{(+1)-(0)}]$	$[Q_{(-1)-(0)}]$	$[Q_{(-1)-(+1)}]$
δR_{12}	0.030	0.027	0.040	−0.003	0.017	0.020	0.003
δR_{23}	0.000	0.001	−0.010	0.001	−0.003	0.003	0.006
δR_{34}	0.016	0.020	0.033	0.004	−0.004	0.008	0.013
δR_{45}	−0.005	−0.007	−0.007	−0.001	−0.002	0.001	0.003
δR_{56}	0.018	0.014	0.017	−0.004	0.011	0.011	0.000
δR_{61}	−0.016	−0.017	−0.024	−0.002	−0.010	−0.011	0.000
δR_{72}	0.000	0.001	−0.010	0.001	−0.003	0.004	0.006
δR_{87}	0.030	0.027	0.040	−0.003	0.017	0.020	0.003
δR_{98}	−0.016	−0.017	−0.013	−0.002	−0.010	−0.011	−0.001
δR_{109}	0.018	0.014	0.017	−0.004	0.011	0.011	0.000
δR_{103}	−0.005	−0.007	−0.006	−0.001	−0.002	0.001	0.003
δR_{17}	−0.024	−0.023	−0.026	0.001	−0.019	−0.017	0.002

[a] δRx_{ij} is the bond length difference expressed in Å between atoms i and j for the molecule defined in Figure 1c.

stylbene-like electron density distribution for each of the two rings and the vinyl group. The LUMO has the electron density distribution of quinoid-type for the central ring with nodes between the vinyl groups, whereas for the ending rings it is similar to the corresponding one of the HOMO. The HOMO−1 electronic density distribution can be considered to be of quinoid character, but with the atomic orbital coefficients for the vinyl groups negligible. Both the cation and anion state wave functions have a contribution of around 98% of their respective SCF reference wave function. Thus, removing or adding an electron from or to O3PV to form the cation or the anion will increase the quinoid character of the central ring, which explains the similarities between the two positive- and negative-charged geometries. The wave function for the first singlet excited state of the neutral O3PV has its main contribution from the configuration resulting by promoting one electron from the HOMO to the LUMO (HOMO, LUMO), and thus the geometry will acquire a quinoid-character for the central ring.

For PER, the HOMO has an electron density distribution forming two distorted naphthalene-like groups with nodes between the carbon atoms connecting them, and the LUMO shows bonding coefficients between the pairs of carbon atoms (1, 6), (3, 4), and (8, 9), as is seen in Figure 3b. HOMO−1 has an electron density distribution resembling the quinoid type, with negligible coefficient contribution for the p_z atomic orbitals of the carbons linking the two moieties. Again, anion and cation forms have very similar structures. The bond length alternation lowers by removing or adding an electron to the system, and there is shortening of the bond lengths between the carbon atoms connecting the two napthalene-like moieties. The first singlet excited state, S_1, has its main contribution from the configuration formed by the single excitation (HOMO, LUMO), and excitation to S_1 leads to very similar changes in the geometry than the ones seen for the anion.

2.1.2. Charge-Transfer Parameters. The small changes in the internal coordinates observed for both O3PV and PER systems mean that there are short paths in the nuclear configuration space necessary to relax the geometry after charge transfer or after reaching the first excited state. These relaxation processes, which require little nuclear rearrangement, should be very fast processes, in accordance with experiments.[1,5,14,24] The energies for O3PV and PER, which are involved in the process of relaxing geometry after adding or removing an electron, are their corresponding internal reorganization energies (λ_i). The values for λ_i calculated using LSDA/4-31G* are shown in Table 3. $\lambda^n(m)$ denotes the λ_i for the process of changing the initial charge of the system m in n units; m and n can be positive or negative. It is seen that for O3PV and PER (at their ground states) the corresponding λ_i's for adding an electron to the neutral form, $\lambda^{+1}(0)$, or to the cation, $\lambda^{+1}(+1)$, and for removing an electron from the neutral form, $\lambda^{-1}(0)$, or from the anion, $\lambda^{-1}(-1)$, are very small. It seems that for PER is easier than for O3PV to remove an electron or to add it. PER would thus on these grounds be a better hole and electron transporter than O3PV. Since $\lambda^{+1}(0)$ are very low, it should be expected then that the mechanisms involved in the electron transfer to a PER or O3PV molecules in its ground state do not have large energy barriers[6] and electron transport might be quite efficient. Assuming the interaction between the states of the donor and the acceptor sites in the composite are large compared with the thermal fluctuations and parabolic potential energy surfaces, the classical ET theory model relates the activation energy E_{act} to the reorganization energy for the ET process by

TABLE 3: Internal Reorganization Energies in eV, λ_i Calculated Using LSDA/4-31G* for O3PV and PER for the Processes of Adding an Electron to the Neutral Form $[\lambda^{+1}(0)]$, Removing an Electron from the Anion $[\lambda^{-1}(-1)]$, Removing an Electron from the Neutral Form $[\lambda^{-1}(0)]$, and Adding an Electron to the Cation $[\lambda^{+1}(+1)]$

system	method	$\lambda^{+1}(0)$	$\lambda^{-1}(-1)$	$\lambda^{-1}(0)$	$\lambda^{+1}(+1)$	EA	IP
	AM1					0.06	8.90
	LSDA/4-31G	0.08	0.07	0.07	0.07	1.29	6.92
O3PV	LSDA/4-31G*	0.08	0.08	0.07	0.06	1.32	6.90
	LSDA/3-21G*	0.10	0.09	0.08	0.08	1.36	7.07
	AM1					0.53	8.60
PER	LSDA/4-31G*	0.04	0.04	0.03	0.04	1.14	7.00
PER	LSDA/3-21G*	0.04	0.03	0.03	0.04	1.25	7.28

$$\Delta E_{act} = \frac{\lambda}{4}\left(1 + \frac{\Delta E^0}{\lambda}\right)^2 \qquad (1)$$

where ΔE^0 is the energy difference between the equilibrium configurations of the final and initial states,[6,8] which is zeroth for self-exchange reactions. The contribution to λ due to the orientation and polarization of surrounding molecules around donor and acceptor sites is not considered here, and λ is the sum of the internal reorganization energies of the two simultaneous processes of removing the charge q from the donor and adding it to the acceptor, $\lambda^{-q}(i) + \lambda^{+q}(j)$, where i and j are the initial charges on the donor and acceptor, respectively.

Applying eq 1 to the charge-transfer processes for the binary systems formed by PER+PER$^+$ and O3PV+O3PV$^+$ for simulating hole transfer, and by PER+PER$^-$ and O3PV+O3PV$^-$

for simulating electron transfer, the values obtained for the activation energy are very small, about 0.02 and 0.03 eV for the hole transfer in PER and O3PV, respectively, and about 0.02 and 0.04 eV for the electron transfer between PER and O3PV molecules, respectively. Given the magnitude of the zero-point energy, this means that these processes do not have a significant barrier to activation, and indeed, PER is a good molecular semiconductor. Where the activation barrier is quite small, such systems can be quite difficult to study theoretically, since nuclear motions have to be treated quantum mechanically. One then has to include the vibrational states in the calculation of the electronic transport.

The electron affinity (EA) and ionization potential (IP) calculated using AM1, and LSDA with different basis sets, are displayed in Table 3. The lack of electron correlation in the AM1 method and the restrictions in basis set keep the electrons tightly bound to the molecule leading to larger IP values and smaller EAs than are seen experimentally. Whereas in the AM1 picture PER is a slightly better acceptor and donor than O3PV, LSDA gives larger IPs and smaller EAs for PER and O3PV. Both components, PER and O3PV, show large electron affinity, and they can act as donors with similar strengths.

The IP(donor)−EA(acceptor) difference is a measure of the standard free energy change that accompanies the electron transfer directly by excitation from the ground state. The process is more favored the smaller is this difference. The LSDA/4-31G* IP(donor)−EA(acceptor) values when O3PV acts as the donor or as the acceptor are very similar, being 5.76 and 5.78 eV, respectively, which is fairly typical of organic systems.[25] This implies that small differences in environment or changes introduced by adding functional groups to the molecules could be used to alter which of the molecules within the binary composite acts as donor or acceptor. Both energy changes for transferring an electron from one molecule to the other is very large, but it should be remembered that the formation of two charged species in close proximity results in a Coulombic stabilization, which should also be considered. Improvement of the composite would involve the lowering of IP(donor)−EA(acceptor) by forming compatible derivatives with suitable donor or acceptor substituents.

2.1.3. Electronic Spectra. As mentioned in the Introduction, radiative and nonradiative decay mechanisms are important in determining the optoelectronic properties since they govern the response of the material to the exciton formed by the irradiation. For optimal photogeneration of charge carriers, the initial exciton should decay to a sufficiently stable state where there is separation of charge to form (e−h) pairs. In this section we investigate the radiative decay mechanisms by calculating the electronic spectra for the isolated molecules. The probability of a radiative transition between two states is related to the spectral intensity, and it is this we focus on in interpreting the spectra. The ZINDO electronic absorption spectra for O3PV, PER, and their respective singly positive and singly negative ions, as well as the first excited state S_1 emission bands, are displayed in Figure 4a,b.

The electronic absorption and emission spectra for the neutral O3PV and PER molecules are in very good agreement with the experimental ones, owing possibly to the major differences in the aggregation state[14,24] due to intermolecular interactions and packing effects. The experimental optical absorption spectrum of PPV shows a strong absorption band between 2.4 and 3.5 eV,[24] and for the three ring's of phenyl-vinylene between 3.0 and 4.0 eV.[24] The optical properties meanwhile of PER are very much dependent on the aggregation state and crystallinity of the sample, or on solvent.[3,4] For example, in *n*-hexane and *n*-octane solvents it absorbs at about 2.90 eV, and the emissions are centered around 2.82 and 2.77 eV, respectively.[14] For both O3PV and PER, the calculated spectra below 6.0 eV involve transitions to low-lying excited states that only involve single excitations between the molecular orbitals. Double excitations lead to excited states of higher energy.

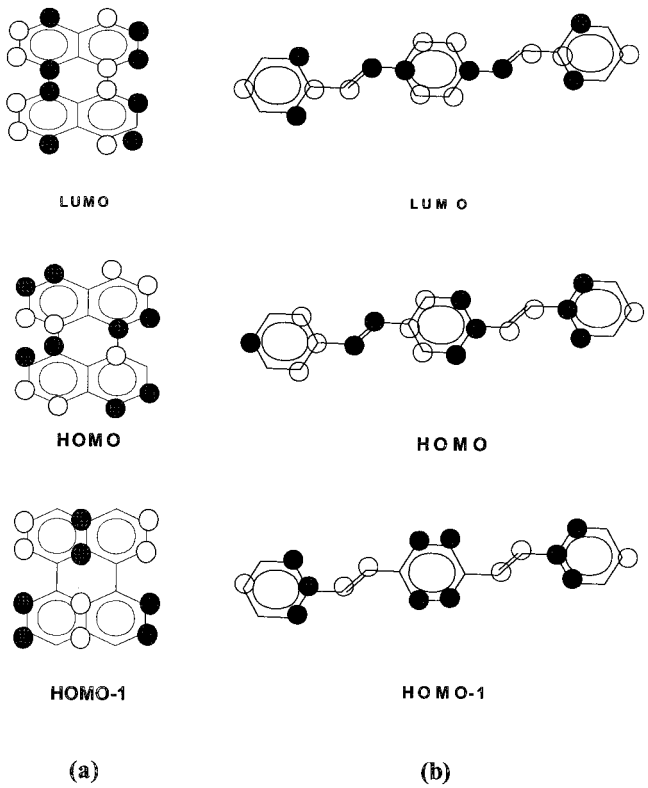

Figure 4. Schematic representation of the vertically ordered HOMO−1, HOMO, and LUMO molecular orbitals (MO) for (a) PER and (b) O3PV systems. The MOs are displayed as a function of the atomic orbital contributions. For simplicity, the size of the atomic orbitals in the figures are not a measure of their corresponding coefficient values, and only atomic orbitals with coefficient larger than 0.2 are displayed.

The O3PV absorption spectrum has an intense band peak centered at about 3.6 eV. This peak is due to the transition $S_0 \rightarrow S_1$, where S_0 represents the ground state and S_1 the first excited state. S_1 has its main contribution from the configuration formed by single excitation from HOMO to LUMO, (HOMO, LUMO). Additionally, another peak appears at about 5.6 eV with significant intensity, about two-thirds of the intensity of the first band, which corresponds to a transition to an excited state generated by several different configurations, which include those generated mainly by single excitations from HOMO−3 to LUMO+3, and from HOMO to LUMO. The electronic absorption spectra bands for the charged species have to be observed if the (e−h) pairs species are created within the composite. The two O3PV charged species, cation $O3PV^+$ and anion $O3PV^-$, both have a medium intensity band centered at about 5.3 eV, overlapping in a large area. PER has a medium intensity absorption peak corresponding to its $S_0 \rightarrow S_1$ transition at about 3.3 eV. S_1 has mainly contributions from configuration (HOMO, LUMO). This peak is much less intense than that associated with the $S_0 \rightarrow S_1$ transition in O3PV. Two other close peaks appear both at about 5.7 and 5.9 eV, respectively, with about double intensity than the $S_0 \rightarrow S_1$ transition. The first peak is associated with the transition to a state formed by several configurations generated mainly by the (HOMO−2, LUMO) and (HOMO, LUMO+2), and (HOMO−1, LUMO)

and (HOMO, LUMO+1), single excitations, and the second peak by the (HOMO−1, LUMO+4) and (HOMO, LUMO+2) single excitations. We observed that there are no important absorptions for the PER cation species in the spectral region between 2 and 6 eV. PER anion absorbs at about 4.8 eV with medium intensity. In the energy region above 5 eV, PER and O3PV charged species absorb more intensely, overlapping with the absorption bands of the neutral PER and O3PV forms.

Relaxing the respective PER and the O3PV S_1 state geometry, the emission spectra bands due to the corresponding $S_1 \rightarrow S_0$ transitions are centered at about 2.9 and 3.0 eV, respectively, in very good agreement with experiments.[3,24] From the equilibrium geometry of the first excited states S_1, in addition to emission, other radiative and nonradiative processes can occur, as it has been experimentally showed that after a short time of irradiation of PPV absorption processes can take place from S_1 in PPV.[24] The calculated absorption spectra from the S_1 states to higher excited states for O3PV and PER are displayed in parts a and b of Figure 1, respectively. They show intense absorption bands appearing above 5.0 eV, overlapping with the O3PV and PER ground-state absorption bands in this energy region. Thus the 5.0−6.5 eV region, which has a high density of electronic states, can be reached by direct photoexcitation from the respective ground states or from the first excited states.

2.2. O3PV+PER System. In a previous work[15] it was seen that O3PV+PER forms a stable molecular system, which has several local structural minima. The separation between O3PV and PER for the most stable AM1 and LSDA/3-21G* structures were about 4.0 and 3.67 Å, respectively. The calculated angle between the O3PV and PER molecular planes was about 70° with O3PV aligned along one of the naphthalene groups of PER, although another minimum only slightly higher in energy was found that had the O3PV molecular rotated 90° around its body-fixed *Z*-axis, keeping its central ring at the same relative position with respect to PER.

AM1 and LSDA/3-21G* calculations showed that the intermolecular interactions are reasonably weak, so that the two molecular components largely retain their molecular characters. Thus the molecular orbitals for the O3PV+PER ground state correspond almost exactly to the molecular orbitals of one or other of its molecular components. At the AM1 equilibrium geometry, the HOMO and LUMO have mainly PER character, whereas HOMO−1, HOMO−2, and LUMO+1 have mainly O3PV character. When O3PV is constrained to be planar, a different vertical ordering in the O3PV and PER character for the occupied molecular orbitals is obtained by LSDA/3-21G*, where HOMO has mainly O3PV character, and HOMO−1 and LUMO, PER character. The unoccupied MOs keep their respective character and ordering for all the nuclear configurations studied. Unfortunately, DFT methods are limited to the study of the ground states, and we cannot do further comparisons between both methods. Keeping in mind that the resulting vertical ordering may be different when using better correlated methods, in what follows we describe the AM1 and ZINDO results, assuming that some of the important semiempirical obtained qualitative descriptions are still valid, such as the weak character of the intermolecular interactions, high preservation of individual component character, geometry trends, relative absorption spectra transition intensities and energies, or associated states. The aspects related to ordering of the MOs, such as possibility of PER acting as a quencher of the O3PV luminescence, have to be taken with caution.

The energies at which the different electronically excited states appear above the ground state, as well as the transition probabilities for reaching the state by photoabsorption, are important factors for the photophysical properties of the system. Both sets of information can be obtained from the electronic absorption spectra. Figure 5 shows the electronic absorption spectra for O3PV+PER at different geometries, where the solid line is the spectra at the optimized ground-state geometry.

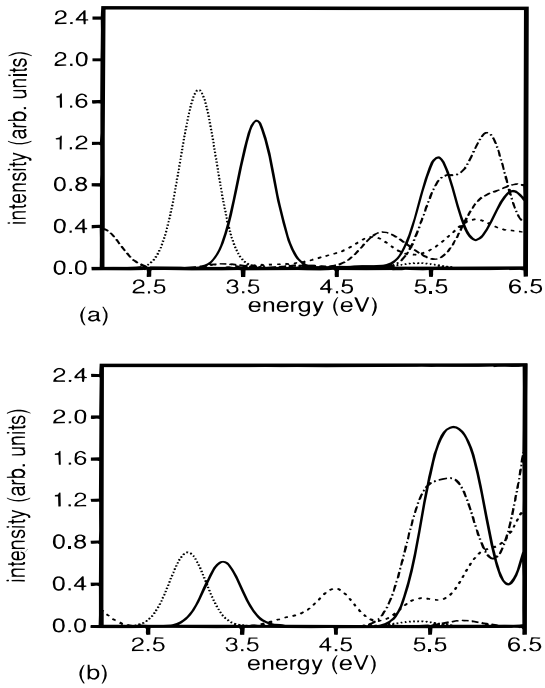

Figure 5. Electronic absorption spectra for the ground states of perylene and O3PV molecules in their neutral (solid line), cation (long-dashed line), and anion (short-dashed line). Electronic emission spectra from the first excited state (dotted line) and electronic absorption spectra of the first excited state (dotted−dashed line). (a) O3PV and (b) perylene. The absorption intensity is given in arbitrary units.

As it was seen in a previous work,[15] there is a strong relationship between the spectra of the supermolecular system and the spectra of the individual components, owing to the relatively weak effect of the intermolecular interactions upon the energy levels of the system. Similarly to the individual components, the excited states that are most important for the photophysical properties of the system are formed by single excitations from the ground state. Configurations generated by double excitations lead to states of higher energy.

Denoting the components PER and O3PV by A and B, respectively, the states that may be reached by photoexcitation with the highest probability and thus have the most intense absorption bands are the $S_1 \equiv S_1(A^*B)$ and $S_2 \equiv S_1(AB^*)$ bands, which lie respectively 3.54 and 4.02 eV above the ground state, and the $S_l(A^*B)$, $S_m(A^*B)$, and $S_n(AB^*)$, which lie at 5.67, 5.83, and 6.05 eV. The state $S_1(A^*B)$ has its major contribution from the configuration formed by the (HOMO, LUMO) single excitation, which $S_1(AB^*)$ has its wave function dominated by the configuration formed from the (HOMO−1, LUMO+1) excitation with a small contribution from the configuration formed by the (HOMO−1, LUMO+2) excitation. The other three higher local excited states studied are generated by a mix of several single excitations. Two of them, $S_l(A^*B)$ and $S_m(A^*B)$, involve mainly PER character molecular orbitals, and the third one, $S_n(AB^*)$, involves molecules orbitals of mainly O3PV character.

The most intense bands correspond to local absorptions within the O3PV component (AB*) in agreement with experiments on

the study of PPV and PER derivative junctions.[5] In this work it is observed as well as that the band corresponding to the excitation $S_0 \rightarrow S_1$ within the PER derivative appears at lower energy than the corresponding PPV band. The $S_0 \rightarrow S_1$ transition (localized on PER) has an intensity that is almost an order of magnitude smaller than the intensity of the strongest band of the spectra due to the transition $S_0 \rightarrow S_2$ (localized on O3PV). The two next higher-lying bands (appearing at about 5.67 and 5.83 eV) are due to local transition on PER and have intensities that are about $^1/_3$ and $^1/_{10}$ of the strongest band, respectively. The second most intense of the absorption bands is due to transition to a state of AB* type and is the one appearing at about 6.05 eV.

The transitions from S_0 to charge-transfer states have very small transition moments (i.e., absorption intensities), and the calculations would indicate that the probability of reaching them directly by photoexcitation is relatively small. We denote by CT_i the singlet charge-transfer states, where *i* is the vertical order within each class, A^-B^+ and A^+B^-. States $CT_1(A^-B^+)$, $CT_1(A^+B^-)$, $CT_2(A^+B^-)$, $CT_2(A^-B^+)$, and $CT_3(A^+B^-)$ lie at 5.28, 5.38, 6.36, 6.40, and 6.57 eV, respectively, (relative to the ground state). The first charge-transfer state, $CT_1(A^-B^+)$, has its wave function composed almost exclusively by the configuration formed by (HOMO−1, LUMO) excitation. The second charge-transfer state $CT_1(A^+B^-)$ meanwhile has its wave function composed mainly by the configuration formed from the (HOMO, LUMO+1) excitation. The next three low-lying charge transfer states studied are generated mainly by single excitations (HOMO−2, LUMO) $[CT_2(A^-B^+)]$, (HOMO, LUMO+2), $[CT_2(A^+B^-)]$, and (HOMO−1, LUMO+3) $[CT_3(A^+B^-)]$.

The local excited states S_1, S_2, S_l, S_m, and S_n, as well as the charge-transfer states, have very small transition moments interconnecting them radiatively, indicating that radiative transitions are likely to be negligible and nonradiative processes should be considered to explain possible pathways connecting these states. Nevertheless, reaching other local excited states higher than S_1 or S_2 might be possible if one thinks of the system as able of performing additional absorption processes from the first local excited state on O3PV, since by comparison with the PPV system, additional absorption is feasible (after a short time of irradiation of PPV, absorption processes from its S_1 state can take place[24]). The first two CT states, each of different type, lie below several local excited states accessible by photoabsorption from the ground state or from the first excited state. From these high-energy locally excited states, it might be possible to reach the CT states via nonradiative decay mechanisms. There is a significant density of excited states mainly comprised of excitations of local character, in the major part concerning excitations within PER, lying between the local excited and charge-transfer states, which may provide ways for nonradiative decay processes through couplings between states at some geometry configurations. Another important feature to the photophysics of the system is that the first triplet excited states of A^-B^+ and A^+B^- are practically degenerate with their corresponding singlet excited states and have very similar geometries. Transitions between states of different spin are forbidden, although impurities can mix the states and relax this selection rule.

Possible nonradiative mechanisms from a given S_1 of the same type, to perform intersystem crossing (ISC) to form a metastable triplet, or to reach another local excited state, S_j, of A*B type through intermolecular energy-transfer mechanisms

$$S_i(AB^*) \rightarrow S_1(AB^*) + \Delta G_{i1}$$

$$S_i(AB^*) \rightarrow T_n(AB^*) + \Delta G_{\mathrm{isc}} \qquad (1)$$

$$\text{or} \quad S_i(AB^*) \rightarrow S_j(A^*B) + \Delta G_{ij(AB^*,A^*B)}$$

or to reach the charge-transfer states through intra- or intermolecular mechanisms

$$S_i(AB^*) \rightarrow CT_j(A^+B^-) + \Delta G_{ij(AB^*,A^+B^-)}$$

$$\text{or} \quad S_i(A^*B) \rightarrow CT_j(A^-B^+) + \Delta G_{i(AB^*,A\text{-}B^+)} \qquad (2)$$

The same holds for the A*B form. S_i can be reached by photoabsorption directly from the ground state or through a nonradiative mechanism, in which case the life time of the state would be longer. These processes can only take place within the short time of the transient species S_i, and thus they are more probable to occur from a triplet or a metastable singlet.

Factors affecting nonradiative processes will affect indirectly the radiative behavior of the system. One of these factors is the relaxation energies implicit when the system has reached a final excited state from an initial state through a nonradiative process. The AM1 relaxation energy for $S_1(AB^*)$ when reached from $S_1(A^*B)$ is about 0.42 eV, and for $S_1(A^*B)$ reached from $S_1(AB^*)$ is about 0.22 eV. The relaxation energy for $CT_1(A^-B^+)$ reached through $S_1(A^*B)$ is about 0.26 eV, and for $S_1(A^*B)$ reached from $CT_1(A^-B^+)$ is about 0.16 eV. It seems that for these cases the system capacity is higher for the process of reaching $CT_1(A^-B^+)$ from $S_1(A^*B)$ and is the lowest in reaching $S_1(A^*B)$ from $S_1(AB^*)$. Low-lying triplet CT states that are quasi-degenerate with their corresponding singlet states and have very similar geometries to the ones of these singlet states would show relaxation energy values for the processes mentioned above coinciding with the ones of the singlet state, with the advantage that they have longer time lifes that allow time enough for the processes to occur.

2.3. Influence of Nuclear Configuration on the Excited States. Electronic coupling between the states involved in the photophysics of the system is evaluated for different geometrical configurations (Q_i), each one corresponding to the equilibrium geometry calculated for each of the states: $S_1(A^*B)$, $S_1(AB^*)$, $CT_1(A^-B^+)$, $CT_1(A^+B^-)$, $S_l(A^*B)$, $S_m(A^*B)$, $S_n(AB^*)$, $CT_2(A^-B^+)$, and $CT_2(A^+B^-)$. These different nuclear configurations are only points in the configurational space **Q**, and they do not follow any reaction path. Upon changes in **Q** the nature of the MOs change, which may be accompanied by a vertical reordering of their energies and may lead to additional mixing between the orbitals of O3PV+PER. To understand the couplings arising from nuclear motion, and geometry changes associated with excitation, we need to calculate how the states mix at the different equilibrium configurations, and we explore this here.

The intermolecular coordinates for the states differ from the corresponding ones of the ground state. For example, for the charge-transfer states considered, the Coulombic interactions lead to shorter distances between donor and acceptor. Nevertheless, we have considered the system to be at the *intermolecular* coordinates obtained for the ground state, since changes in the relative spatial coordinates of the molecular components in the solid state are expected to be negligible during the time the photophysical processes of interest take place. Thus, in what follows, we only optimize for each state the internal coordinates of each of the molecular components.

TABLE 4: AM1 Bond Lengths Obtained for the Component O3PV in the Composite O3PV+PER for the Ground State [S_0], the First Singlet and Triple Excited States for A*B, the First Singlet Excited State for AB*, the First Singlet and Triple Excited States for A^-B^+, and the First Singlet Excited State for A^+B^- [a]

system	S_0	S_1(A*B)	T_1(A*B)	S_1(AB*)	$S_1(A^-B^+)$	$T_1(A^-B^+)$	$S_1(A^+B^-)$
Ra_{12}	1.396	1.396	1.396	1.397	1.397	1.396	1.393
Ra_{23}	1.387	1.389	1.386	1.384	1.389	1.388	1.397
Ra_{34}	1.406	1.405	1.407	1.413	1.408	1.408	1.388
Ra_{45}	1.401	1.401	1.401	1.408	1.402	1.402	1.413
Ra_{56}	1.397	1.394	1.395	1.397	1.399	1.395	1.397
Ra_{61}	1.396	1.396	1.396	1.397	1.397	1.396	1.393
Re_{17}	1.451	1.453	1.450	1.430	1.448	1.446	1.446
Re_{78}	1.343	1.343	1.343	1.372	1.353	1.355	1.353
Re_{81}	1.455	1.453	1.450	1.414	1.437	1.446	1.432
Rb_{12}	1.402	1.405	1.404	1.428	1.417	1.417	1.418
Rb_{23}	1.392	1.390	1.391	1.371	1.380	1.380	1.373
Rb_{34}	1.402	1.404	1.403	1.427	1.420	1.420	1.421
Rb_{45}	1.406	1.407	1.407	1.428	1.435	1.434	1.423
Rb_{56}	1.389	1.389	1.388	1.369	1.370	1.370	1.373
Rb_{61}	1.402	1.405	1.404	1.428	1.417	1.417	1.418

[a] A represents the PER molecule and B the O3PV. Rx_{ij} is the bond length in Å between atoms i and j for the unit cell x as defined in Figure 1b.

TABLE 5: AM1 Bond Lengths Obtained for the Component PER in the Composite O3PV+PER for the Ground State [S_0], the First Singlet and Triple Excited States for A*B, the First Singlet Excited State for AB*, the First Singlet and Triple Excited States for A^-B^+, and the First Singlet Excited State for A^+B^- [a]

system	S_0	S_1(A*B)	T_1(A*B)	S_1(AB*)	$S_1(A^-B^+)$	$T_1(A^-B^+)$	$S_1(A^+B^-)$
R_{12}	1.385	1.415	1.432	1.392	1.404	1.405	1.429
R_{23}	1.432	1.424	1.423	1.430	1.428	1.427	1.427
R_{34}	1.419	1.431	1.438	1.422	1.431	1.431	1.387
R_{45}	1.421	1.412	1.406	1.420	1.414	1.413	1.393
R_{56}	1.372	1.388	1.402	1.375	1.383	1.385	1.424
R_{61}	1.411	1.390	1.374	1.405	1.391	1.391	1.407
R_{ab}	1.459	1.435	1.417	1.453	1.440	1.441	1.434

[a] A represents the PER molecule and B the O3PV. R_{ij} is the bond length in Å between atoms i and j for the unit cell x as defined in Figure 1c.

Tables 4 and 5 show the equilibrium geometries for different excited states of the moieties of the system, O3PV and PER, respectively. For all the states, the geometry of the terminal rings of the O3PV remains fairly unchanged from that of the ground state. Most of the geometry changes in O3PV affect the central ring and the vinylene groups, mainly in the CC bond lengths. For the S_1(A*B) state's equilibrium geometry (denoted as $\mathbf{Q}_1$(A*B), only the PER component is significantly affected, possessing a geometry very similar to that of the first excited state of the isolated PER molecule.

At this equilibrium geometry, together with the ones corresponding to $CT_1(A^-B^+)$ and $CT_1(A^+B^-)$ states ($\mathbf{Q}_1(A^-B^+)$ and $\mathbf{Q}_1(A^+B^-)$, respectively), the HOMO−1, HOMO, LUMO, and LUMO+1 show the same local character nature (O3PV, PER, PER, and O3PV, respectively) than the ones of the ground-state geometry, $\mathbf{Q}_0$. This would indicate that the electronic coupling between the different molecules has a similar nature to that of the ground state, and it is relatively weak.

At $\mathbf{Q}_1$(A*B), the energetic ordering of the states is such that the first local excited state on O3PV is no longer the second excited state of the system but lies instead above other excited states of A*B type. The existence of these lower-lying PER local excited states would increase the probability of quenching of O3PV luminescence by PER.

The $\mathbf{Q}_1$(AB*) equilibrium geometry configuration, which corresponds to the first O3PV local excited state, is the one that differs the most with respect to $\mathbf{Q}_0$. These differences are mainly on the O3PV, although there are structural changes in PER as well. The energy difference for state S_1(AB*) with respect to the ground state lowers only by about 0.02 eV. The equilibrium geometry for this state is expected to be reached within the picosecond time scale, since it has been seen experimentally that the luminescence of PPV from its first excited state is very efficient and occurs within a few picoseconds. This is an important observation since we see significant changes in MOs at the $\mathbf{Q}_1$(AB*) geometry.

At the $\mathbf{Q}_1$(AB*) and $\mathbf{Q}_l$(A*B) equilibrium geometrical configurations, the HOMO, HOMO−1, LUMO, and LUMO+1 have mainly the local characters of PER, O3PV, PER, and O3PV, respectively, which is an energy ordering expected to favor charge transfer over energy transfer.

Changes in the PER and O3PV character of the MOs at $\mathbf{Q}_1$(AB*) and $\mathbf{Q}_n$(AB*) reflect strong mixing between states. The mixing is seen to be between local excitation states of different type, A*B and AB*, and coupling between both local excitation and ionic pair radical kind states, as for example AB* and $CT_2(A^-B^+)$, and A*B, AB*, and $CT_2(A^+B^-)$ couplings.

At the charge-transfer A^-B^+ equilibrium internal configuration, $\mathbf{Q}_1(A^-B^+)$, the states of the form A^-B^+ show strong interaction with A*B type states, which may indicate that $Q_1(A^-B^+)$ is near a region where $CT_1(A^-B^+)$ and S_1(A*B) couple effectively. At $\mathbf{Q}_1(A^+B^-)$ there is a strong mixing between local-excited states, in particular S_1(A*B) and S_2(AB*).

It seems that changes in coordinates on the O3PV component are decisive in generating strong interactions between the states, that is, $\mathbf{Q}_1$(AB*) is favorable for interactions between states. Other excited states than the ones under study also participate in these couplings. Regions in the **Q** space where two (or more) states show strong coupling with each other can be identified as regions near avoided crossing hypersurfaces between the respective potential energy surfaces of the interacting states. The existence of these regions and the high density of states actively coupling with one another is a very important factor that affects the photophysics of the system by the enhancement of nonradiative processes.

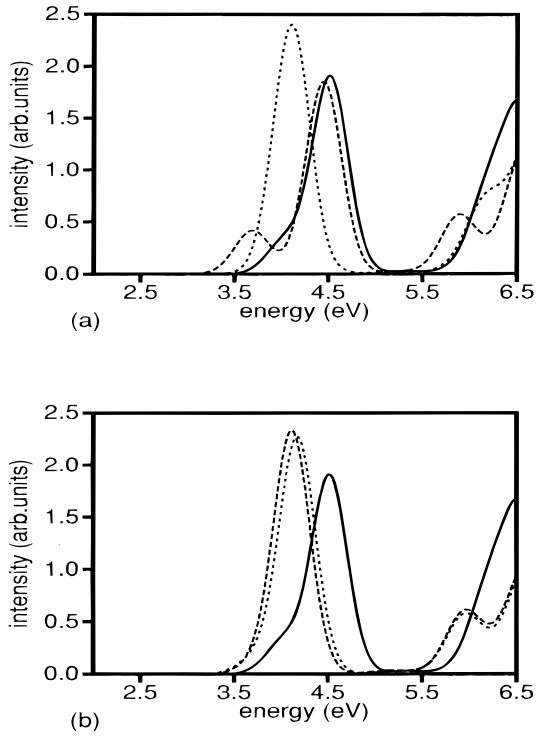

Figure 6. Electronic absorption spectra for the O3PV+PER system at various geometry configurations **Q**: (a) for the geometries of the ground state (solid line), the first local excited state on PER (dashed line), and the first local excited state on O3PV (dotted line) geometries, and (b) for the geometries of the ground state (solid line), the first charge-transfer state of the form A^-B^+ (dashed line), and the first charge-transfer state of the form A^+B^- (dotted line) geometries. A stands for PER and B for O3PV.

Changes of the nature of the excited states can be observed additionally from the analysis of the absorption spectra for the system at the different internal geometry configurations. The electronic absorption spectra for O3PV+PER at $\mathbf{Q}_0$ (ground state), $\mathbf{Q}_1$(A*B), and $\mathbf{Q}_1$(AB*) are displayed in Figure 6a, and at $\mathbf{Q}_0$, $\mathbf{Q}_1(A^-B^+)$, $\mathbf{Q}_1(A^+B^-)$, in Figure 6b.

At $\mathbf{Q}_1$(A*B) the spectra shows a better separation for the bands of $S_0 \rightarrow S_1$ and $S_0 \rightarrow S_2$ transitions than the corresponding ones at $\mathbf{Q}_0$. The peak of the $S_0 \rightarrow S_l$(A*B) transition is shifted to lower energies and shows a slightly larger intensity than it does at the $\mathbf{Q}_0$ configuration. The peak of the $S_0 \rightarrow S_m$(AB*) transition shifts to higher energies, and their intensities diminish by one-half. All this is in agreement with our previous result, which indicated only weak interactions between states at the equilibrium geometry of the PER locally excited state, $\mathbf{Q}_1$(A*B), and only A*B type states were stabilized, with the first O3PV local excited state becoming more unstable.

At $\mathbf{Q}_1$(AB*) the two bands due to the transitions $S_0 \rightarrow S_1$ and $S_0 \rightarrow S_2$, are broader, which reflects larger overlap between MOs and an increase in the number of states accessible by photoexcitation.

In general it is seen that for each $\mathbf{Q}_i$ the $S_0 \rightarrow S_2$ transition shows comparable absorption intensity, and the $S_0 \rightarrow S_n$ transition (localized on O3PV) has the largest absorption intensity, which suggests that O3PV is more active than PER for absorbing photons.

The similarity between the absorption spectra from the ground state at geometries $\mathbf{Q}_1(A^-B^+)$ and $\mathbf{Q}_1(A^+B^-)$ is a consequence of the similar geometries for the singly negative and singly positive charged species. $\mathbf{Q}_1(A^-B^+)$ and $\mathbf{Q}_1(A^+B^-)$ are very close points in the **Q** space, i.e., almost negligible geometry relaxation is needed to reach one state from the other, which may be important in the photophysics of the system.

3. Discussion and Conclusions

In this study we have attempted to examine the perylene and poly(*p*-phenylenevinylene) composite, taking a molecular system as a model. Owing to the relatively large size of this system, our study has been principally restricted to using semiempirical methods, which we hope capture the essential physics of these materials and provide a basis for future ab initio calculation. Using AM1 with full posterior configuration interaction within an active space of 10 π orbitals and the ZINDO method, we have identified important electronic states that may be associated with its photoconductive properties and have additionally calculated parameters from classical electron-transfer theory that may be useful in understanding charge transport in these types of materials.

The calculated internal reorganization energies for electron-transfer processes at the ground state for the two components imply that PER is a slightly better hole and electron transporter than O3PV, although for both components, the charge carrier transport process seems to occur practically without barrier, given the likely magnitude of the zero-point energy, at the calculated equilibrium geometry of the ground state.

A composite formed by PER and O3PV is not expected to have the best performance as photogenerator of charge carriers, since the PER and O3PV capacities to act as acceptors or donors are quite similar. Improvement of the composite would involve the lowering of the IP(donor)−EA(acceptor) differences by forming compatible derivatives with suitable donor or acceptor substituents.

In the composite the most intense band corresponds to the first local absorption within the O3PV component, i.e., O3PV is the component that is the most probable to be photoexcited. The calculations show the first CT states (of the form A^-B^+ and A^+B^-) to be lower in energy than the local excited states on O3PV and PER, which have the most intense absorptions. There is also a significant density of electronic states of local character, in major part within component PER, which are not reached by direct photoexcitation from the ground state but by photoexcitation from the first and second local excited states (of form A*B and AB*, respectively). These states may provide ways for nonradiative processes through strong couplings between states at certain geometrical configurations. Radiative and nonradiative processes would lead to intermediate states from which charge-transfer processes can occur thanks possibly to the triplet states.

It seems that changes in configuration of the O3PV component is a decisive factor for providing important changes in the electronic structure of the system. At the equilibrium geometry of the first local excited state within O3PV, $\mathbf{Q}_1$(AB*), which is expected to be reached very fast, important coupling between states appear, mixing A*B and AB* character, and ionic and exciton character of several states.

It is important to remember that this is a qualitative study of the system using quantum chemistry methods. A better description of the system may give some vertical reordering between the different states, and some possible radiative and nonradiative mechanisms may change with respect to the AM1/ZINDO picture. Nevertheless, important features for its photophysics may not vary significantly, such as their relative absorption and emission intensities of the electronic spectra, the nature of the most probable states to be reached upon radiating the system (still to be of local character within O3PV) that will be kept, or

the important fact that the charge-transfer states seems not be reacheable by photon excitation from the ground state of the system.

In our calculations we obtained a high energy difference between the charge-transfer states and the ground-state energy at the ground-state equilibrium configuration $\mathbf{Q}_0$, which is questionable. This may be a consequence of the fact that charge-transfer states are less accurately described by the methods used in this work than the local excited states. In the local excited state additional interactions appear owing to electronic polarization. This effect is even larger in ionic states. AM1/ZINDO methods underestimate the overall energy difference between the excited states and the ground state since it underestimates the interactions characteristic of open shells. They do not properly account for very polar states and Coulombic interactions in ion pair radicals. A more relevant description of the system would most probably result in a much lower excitation energy differences for the CT states with respect to the ground state. The inclusion of other factors such as an applied external electric field will also favor the system reaching CT states as a consequence of the high polarizability of these systems.

Another factor to take into account is the distance and orientation between the components within the system. The Coulombic forces stabilize the ion pair states as the distance between donor and acceptor disminishes, and a proper consideration of the molecular packing in these materials may be needed. An efficient packing would stabilize the separate charge and inhibit earlier recombination and, thus, lead to better carrier generation efficiencies. As it is shown in the diagram in Figure 2, it can be found a configuration in **Q** space at which the potential energy surfaces between a local excited state and a CT state cross, and a region at which the CT state is more stable than the local excited state. In additional calculations at shorter distances, 3.5 and 3.0 Å, and with molecular planes in parallel, a large mixing of PER and O3PV MOs forming the PER+O3PV MOs is observed.

Distance is a relevant factor as well in ET theory, as for example, the ET coupling integral between the two states involved in the electron transfer depends approximately exponentially on the donor−acceptor distance.[8,31]

Our study of the energy and characteristics of the different excited states showed that the different geometrical internal configurations of the system, which span the $\mathbf{Q}_0$ space, play an important role in the photophysics of the system. The ground-state equilibrium configuration is important for determining the photophysical processes of photon absorption. After photon absorption, the different possible competitive photophysical mechanisms, radiative and nonradiative, can be strongly affected by the different internal geometry configurations, since vertical reordering of the energy of the states and/or changes in their nature can be very significant.

At the O3PV local S_1 equilibrium geometry, $\mathbf{Q}_1$(AB*), the interactions between both components of the system becomes more important. The system shows a mixing of local excitation and ionic pair radical character MOs; the system is close to a crossing point between the potential surfaces corresponding to a local excited state and a charge-transfer state.

The energy involved in the process of geometry relaxation, once the system is in one of the first local excited states—PER or PPV—is very small, and the nuclear coordinate changes that the system should undergo to reach the minimum of the respective excited states are additionally quite small, which suggests that this minima can be reached very fast, in agreement with experiments on PPV.

All this, together with the fact that the activation energies, obtained by applying eq 1 to the charge-transfer processes, are very small, suggest that a possibility of reaching a CT state by an ET mechanism, assisted by internal coordinate changes in the components with no need of changes in the intermolecular coordinates for the system, once the system is at the O3PV first excited state geometry, would be relatively favorable and fast.

This may suggest a possible mechanism for the system to undergo charge separation that first the system at $\mathbf{Q}_0$ is excited mainly to a O3PV moiety, the system relaxes to the first O3PV local excited state, and it reaches the equilibrium $\mathbf{Q}_1$(AB*) configuration within few picoseconds. At this geometry it is possible for the system to reach a CT state very quickly by a simple ET mechanism. This process may be enhanced by, for example, applying an external electric field, by forming suitable derivatives for O3PV and PER that make them better acceptor and donor, respectively, or by more efficient packaging.

Acknowledgment. The author is grateful for support from the Belgian Prime Minister's Office of Science Policy "Pôle d'Attraction Interuniversitaire. Phase IV", and would also thanks Dr. Andrew Meredith for discussions, and the appreciable help received from the group of Prof. Jean-Luc Brédas.

References and Notes

(1) See, for example: (a) Tang, C. W. *Appl. Phys. Lett.* **1986**, *48*, 183. (b) Horowitz, G.; Fouki, F.; Spearman, P.; Fichon, D.; Nogues, C.; Pan, X.; Garnier, F. *Adv. Mater.* **1996**, *8* (3), 242. (c) Steren, C. A.; van Willigen, H.; Biczók, L.; Gupta, N.; Linschitz, H. *J. Phys. Chem.* **1996**, *100*, 8920. (d) Saricifti, N. S.; Smilovitz, L.; Heeger, A. J. *Science* **1992**, *258*, 1474.

(2) Yu, G. *Synth. Met.* **1996**, *80*, 143−150.

(3) See, for example: Law, K.-Y. *Chem. Rev.* **1993**, *93*, 449.

(4) Gregg, B. A. *J. Phys. Chem.* **1996**, *100*, 852.

(5) Halls, J. J. M.; Friend, R. H. *Synth. Met.* **1997**, *85*, 1307.

(6) (a) Marcus, R. A. *Ann. Rev. Phys. Chem.* **1964**, *15*, 155. (b) Markus, R. A. *J. Phys. Chem.* **1956**, *24*, 966. (c) Levich, V. G. *Adv. Electrochem. Eng.* **1965**, 4249. (d) Hush, N. S. *Trans. Faraday Soc.* **1961**, *57*, 557. (e) Hush, N. S. *Electrochim. Acta* **1965**, *13*, 1005. (f) Gloss, G. L.; Miller, J. R. *Science* **1988**, *240*, 440. (g) Wasielewski, M. R. *Chem. Rev.* **1992**, *92*, 435. (h) Conolly J.; Bolton, J. R. *Photoinduced Electron Transfer*; Fox, M. A., Chanon, M., Eds.; Elsevier: Amsterdam, 1988; Part D. (i) Liang, C.; Netwon, M. D. *J. Phys. Chem.* **1992**, *96*, 2855.

(7) Larsson, S. *Int. J. Quantum Chem.* **1986**, *30*, 31.

(8) Rodriguez-Monge, L.; Larsson, S. *J. Chem. Phys.* **1995**, *102*, 7106.

(9) Baigent, D. R.; Holmes, A. B.; Moratti, S. C.; Friend, R. H. *Synth. Met.* **1996**, *80*, 119.

(10) Greenham, N. C.; Samuel, I. D. W.; Hayes, G. R.; Philips, R. T.; Kessever, Y. A. R. R.; Moratti, S. C.; Holmes, A. B.; Friend, R. H. *Chem. Phys. Lett.* **1995**, *241*, 89.

(11) Ashwell, G. J.; Jefferies, G.; Hamilton, D. G.; Lynch, D. E.; Roberts, M. P. S.; Bahra, G. S.; Brown, C. R. *Nature* **1995**, *375*, 385.

(12) Park, J. Y.; Le, H. M.; Kim, G. T.; Park, H.; Park, Y. W.; Kang, I. N.; Hwang, D. H.; Shim, H. K. *Synth. Met.* **1996**, *79*, 177.

(13) Janssen, R. A. J.; Sariciftci, N. S.; Heeger, A. J. *J. Chem. Phys.* **1994**, *100* (12), 8641.

(14) (a) Jiang, Y.; Blanchard, G. J. *J. Phys. Chem.* **1994**, *98* (38), 9419. (b) Jiang, Y.; Blanchard, G. J. *J. Phys. Chem.* **1994**, *98* (26), 6437. (c) Joblin, C.; Salama, F.; Allamandola, L. *J. Chem. Phys.* **1995**, *102* (24), 9743.

(15) Rodriguez-Monge, L.; Brédas, J.-L. To be submitted.

(16) Dewar, M. J. S.; Zoebisch, E. G.; Healy, E. F.; Steward, J. J. P. *J. Am. Chem. Soc.* **1985**, *107*, 3902.

(17) Mao, G.; Fisher, J. E.; Karasz, F. E.; Winokur, M. J. *J. Chem. Phys.* **1993**, *98*, 712.

(18) Ridley, J.; Zerner, M. C. *Theor. Chim. Acta* **1973**, *32*, 111.

(19) Mataga, N.; Nishimoto, K. *Z. Phys. Chem.* **1957**, *13*, 140.

(20) Hehre, W. J.; Steward, R. F.; Pople, J. A. *J. Chem. Phys.* **1969**, *51*, 2657.

(21) (a) Khon, W.; Sham, L. J. *Phys. Rev.* **1965**, *140*, A1133. (b) Vosko, S. H.; Wilk, L.; Nusair, M. *Can. J. Phys.* **1980**, *58*, 1200.

(22) Binkley, J. S.; Pople, J. A.; Heher, W. J. *J. Am. Chem. Soc*. **1980**, *102*, 939.

(23) Ditchfield, R.; Hehre, W. J.; Pople, J. A. *J. Chem. Phys.* **1971**, *56*, 724.

(24) Cornil, J.; Beljonne, D.; Shuai, Z.; Hagler, T. W.; Campbell, I.; Bradley, D. D. C.; Brédas, J.-L.; Spangler, C. W.; Mülen, K. *Chem. Phys. Lett.* **1995**, *247*, 425.

(25) Bhattacharyya, K.; Chowdhury, M. *Chem. Rev.* **1993**, *93*, 507.

(26) Bradley, D. D. C. *Synth. Met.* **1993**, *54*, 401.

(27) (a) Tang, C. W.; VanSlyke, S. A. *Appl. Phys. Lett.* **1987**, *51*, 913. (b) Tang, C. W.; VanSlyke, S. A.; Chen, C. H. *J. Appl. Phys.* **1989**, *65*, 3610.

(28) Weaver, M. S.; Bradley, D. D. C. *Synth. Met.* **1996**, *83*, 61.

(29) Bradley, D. D. C. *J. Phys. D: Appl. Phys*. **1987**, *20*, 1389.

(30) Lhost, O.; Bredas, J. L. *J. Chem. Phys.* **1992**, *96* (7), 5279.

(31) Rodriguez-Monge, L.; Larsson, S. *J. Phys. Chem.* **1996**, *100* (15), 6298. Rodriguez-Monge, L.; Larsson, S. *J. Chem. Phys.* **1996**, *105* (17), 7857. Rodriguez-Monge, L.; Larsson, S. *Int. J. Quant. Chem.* **1997**, *61*, 847.